Wireless Non-Floating Type Thermal Bubble Accelerometer with Semi-Cylindrical Chamber

JIUM-MING LIN AND PO-KUANG CHANG
Ph.D. Program in Engineering Science, College of Engineering
Chung-Hua University
707, Sec. 2 Wu-Fu Rd. Hsin-Chu
TAIWAN, R. O. C.
jmlin@chu.edu.tw http://www.cm.chu.edu.tw/files/11-1017-2419.php

Abstract: - This research proposes a wireless RFID-based thermal bubble accelerometer design, and relates more particularly for the technology to manufacture and package it on a flexible substrate. The key technology is to integrate both a thermal bubble accelerometer and a wireless RFID antenna on the same substrate, such that the accelerometer is very convenient for fabrication and usage. In this paper the heaters as well as the thermal sensors are directly adhering on the surface of the flexible substrate without the traditional floating structure. Thus the structure is much simpler and cheaper for manufacturing, and much more reliable in large acceleration impact condition. In addition, the shape of the chamber is changed as a semi-cylindrical or semi-spherical one instead of the conventional rectangular type. Comparisons are also made; one can see the sensitivity of the proposed new shape design is better.

Key-Words: - Wireless RFID Tag, Thermal Bubble Accelerometer, Flexible Substrate, Thermal Sensor, Heater, E-beam Evaporation, Thermal Piles, Polysilicon Doped with P-type Impurity.

1 Introduction

Conventional thermal bubble accelerometers are manufactured on silicon wafers [1-13], and the chamber is filled with air or carbon dioxide [2-6]. The key technology of this paper is to integrate both a thermal bubble type accelero-meter and a wireless RFID antenna on the same flexible substrate as in Fig. 1, such that it is very convenient for fabrication and usage. The proposed accelerometer is manufactured on a flexible substrate such as plastic or PET film, which is obtained by low temperature deposi-tion process to make the heater as well as temperature sensors at either side. The heater is made by Cr and Ni with E-beam evaporation. The temperature sensors can be either made by polysilicon doped with P-type impurity such as boron, or obtained by the same E-beam evapo-ration process as heater with K-type (Chromel and Alumel), J-type (Iron and Cons- tantan), E - type (Chromel and Constantan) and T-type (Copper and Constantan) thermal piles.

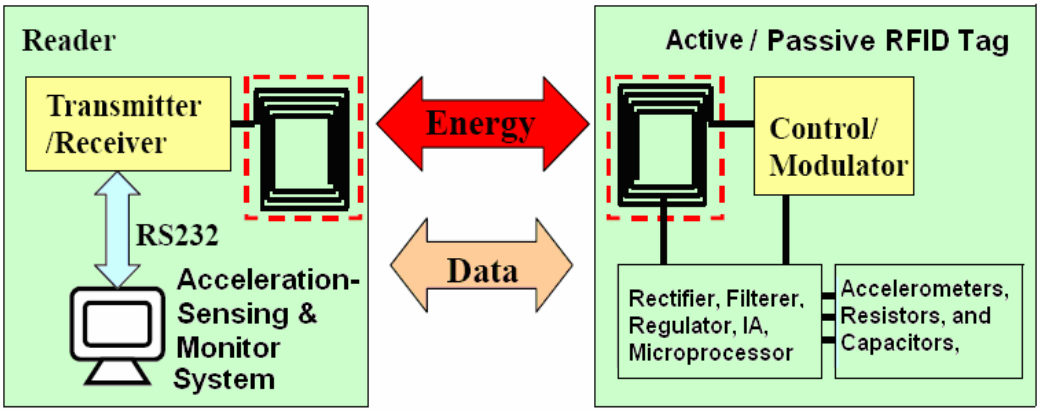

Fig.1. The block diagram of the wireless RFID-based thermal bubble type accelerometer module.

The most distinguished one is that the proposed device directly adheres on the substrate without making the floating structure; thus it will increase the reliability as well as decrease the cost of fabrication. By the way the chamber is filled with inert gas such as Xe or Ar to avoid the oxidizing effect produced by the previous commercial ones with carbon dioxide or air that will reduce the reliability as well as the life cycle of the heater. In addition, the internal shape of the chamber uses semi-cylindrical one to speed up the fluid flow for heat convection such that the bandwidth of the new structure is larger than the traditional one with rectangular package [7]. On the other hand the outer shape of the package uses the rectangular type for easy marking the part and series numbers. Finally, the device is also augmented with RFID tag technique to make the accelerometer as a wireless one for easy application in various fields, such as sports, hospital monitoring, air bag, game, remote navigation and guidance, exercising, etc. Comparisons with the conventional thermal bubble accelerometer with rectangular chamber and filled with carbon dioxide are also made. We have shown that the sensitivity of the newly proposed semi-cylindrical chamber is better. The paper organization is as follows: the first section is introduction. The second one is fabrication and packaging steps. The third one is simulation results and discussion. The last part is the summary.

2 Fabrication and Packaging Steps

Step 1: Evaporate S_iO_2 on both sides of substrate for thermal, electrical and humidity isolation. The next is to cover Photo Resist (PR) on both sides to protect the layers of S_iO_2. The result is in Fig. 2.

Fig.2. The result of design Step 1.

Step 2: Covering a layer of SU-8 PR at the front side. Then using mask #1 and Photo-lithography And Etching Processes (PAEP), a cavity is formed on the substrate. The result is in Fig.3.

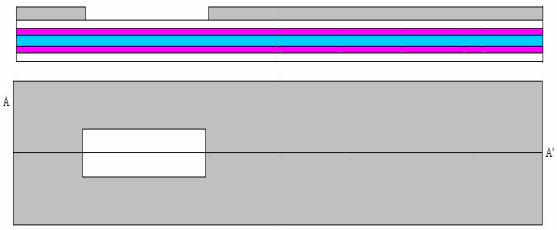

Fig.3. The result of design Step 2.

Step 3: Evaporate S_iO_2 on the front side of substrate as the sacrificial layer; the thickness is about one half of the SU-8 layer. The next is to cover a layer of PR on the front side. Using mask #1 and PAEP, the PR on the cavity is remained to protect the under lying layer of S_iO_2. Then remove the layer of S_iO_2 around the cavity. The result is in Fig.4.

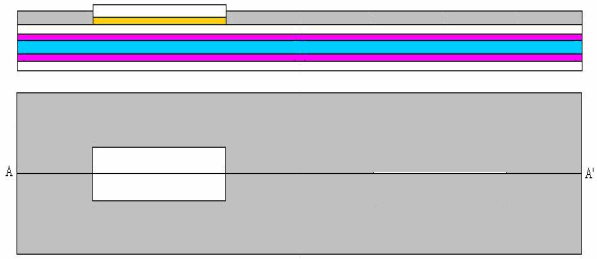

Fig.4. The result of design Step 3.

Step 4: Remove PR on the cavity, and the chamber is obtained. Evaporate a layer of alumina oxide to support the heater and temperature sensors. Covering the front side with SU-8 PR, and using mask #2 and PAEP, only the PR on the cavity is left on the substrate to protect the under lying layer of alumina oxide. The result is in Fig.5.

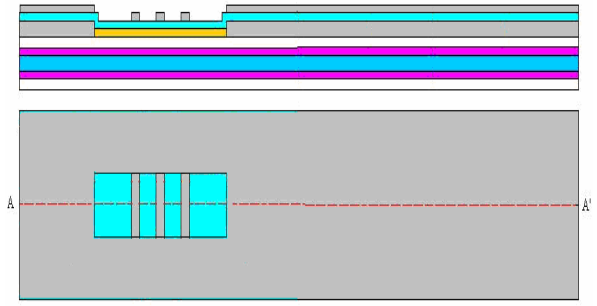

Fig.5. The result of design Step 4.

Step 5: By E-gun evaporator deposit a layer of p-type amorphous silicon with thickness 100-250 μm, then using an Nd-YAG laser to anneal it as a poly-silicon thermister. The next is to use mask #3 and PAEP to reserve the PR on the poly-silicon thermister. Finally, use KOH solution or RIE process to remove the layers of poly-silicon without PR protection. After remove the PR, the result is in Fig.6.

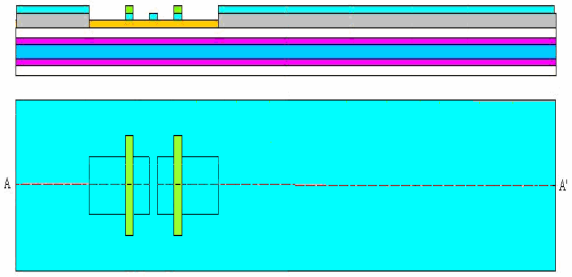

Fig.6. The result of design Step 5.

Step 6: By E-gun evaporator deposit respectively a layer of Cr and Ni to be used as heater, RFID antenna, as well as the conductors connected to the power supply. The next is to use mask #4 and PAEP to reserve the PR on the heater, RFID antenna, as well as the conductors connected to the power supply. Finally, use sulfuric acid solution or RIE process to remove the layers of Cr and Ni without PR protection.

After remove the PR, the result is in Fig.7. Note that the temperature sensors can also be made by the E-beam evaporation process by using one set of the thermal pile materials as follows: K-type (Chromel and Alumel), J-type (Iron and Constantan), E -type (Chromel and Constantan) and T-type (Copper and Constantan).

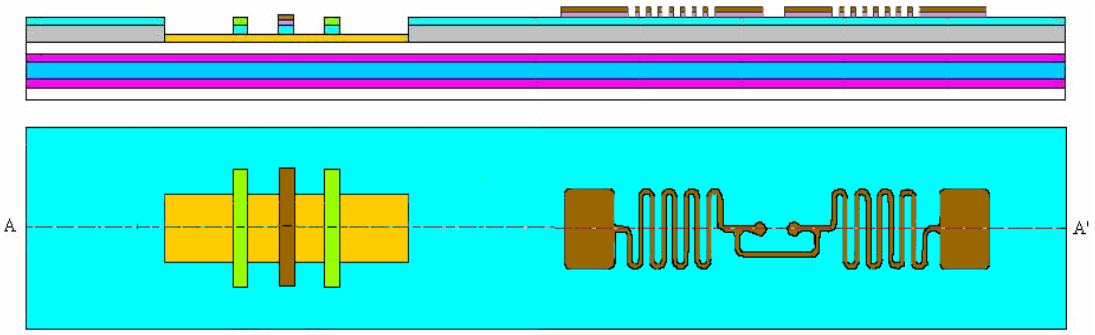

Fig.7. The result of design Step 6.

Step 7: Using mask #5 and PAEP to reserve the PR on the heater, and then flash a layer of gold on the layer Ni by electroless-plating. Thus the conductivity of the RFID antenna, as well as the conductors connected to the power supply would be very good. Besides, the performance of the soldering process on the pads would also be increased, the result is in Fig.8.

Step 8: Covering PR on the front side. Using mask #2 and PAEP to make the silicon dioxide layer at the chamber uncovered by the PR. Then remove the dioxide layer at the chamber uncovered by the PR. Thus the heater as well as the thermisters can be released, the result is in Fig.9.

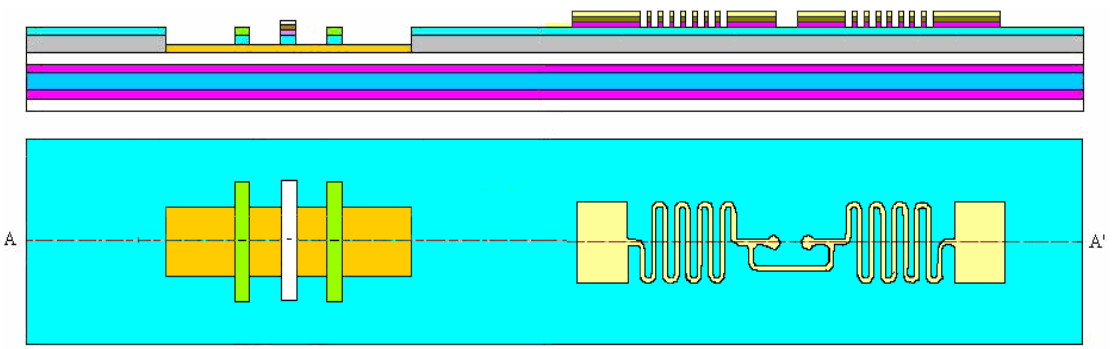

Fig.8. The result of design Step 7.

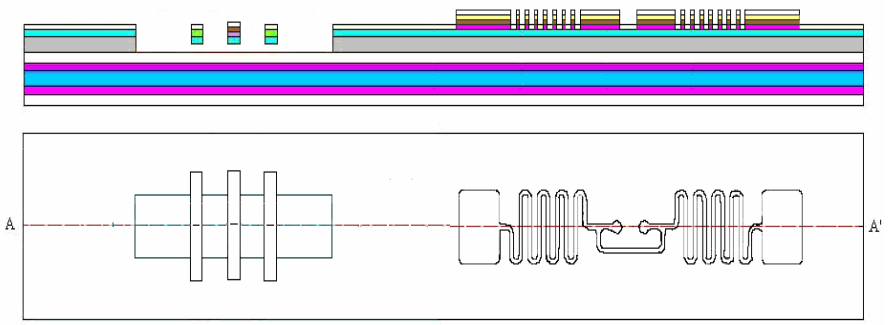

Fig.9. The result of design Step 8.

Step 9: Remove the photo resist on the substrate, and using screen printing method to put plastic or polymer as the sealing material around the accelerometer as dam bar, and the chip with metal bump is flip chip bonded to the RFID feed terminal by thermal compression method, then make the underfill to increase the adherence of chip. Finally, put a cap with semi-cylindrical or semi-spherical shaped internal chamber on the dam bar, before curing and sealing it one can fill it with the traditional carbon dioxide or the proposed xenon gas, and the result is in Fig.10.

Step 10: To increase the sensitivity as well as reducing the drift and bias effects due to fabrication errors, we put four accelerometers in a full differential Wheatstone bridge structure. Putting a socket and a spring for fixing the battery on the substrate, the result is in Fig.11.

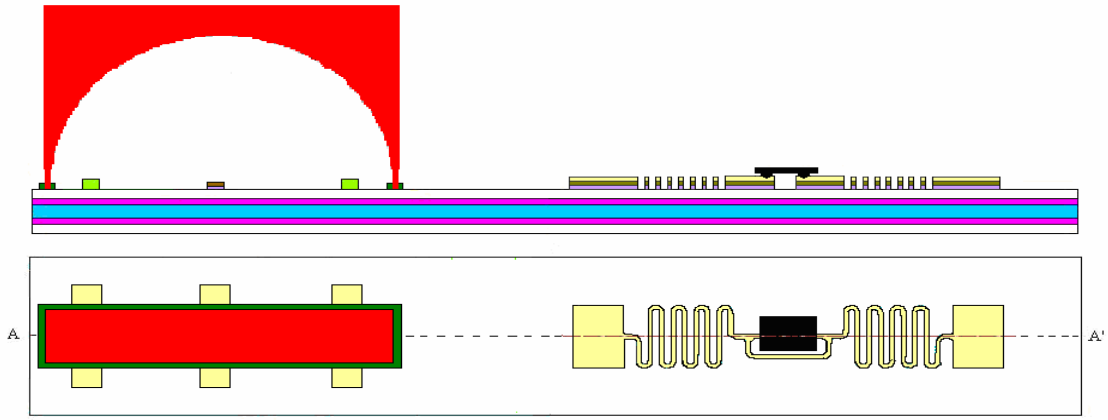

Fig.10. The result of design Step 9.

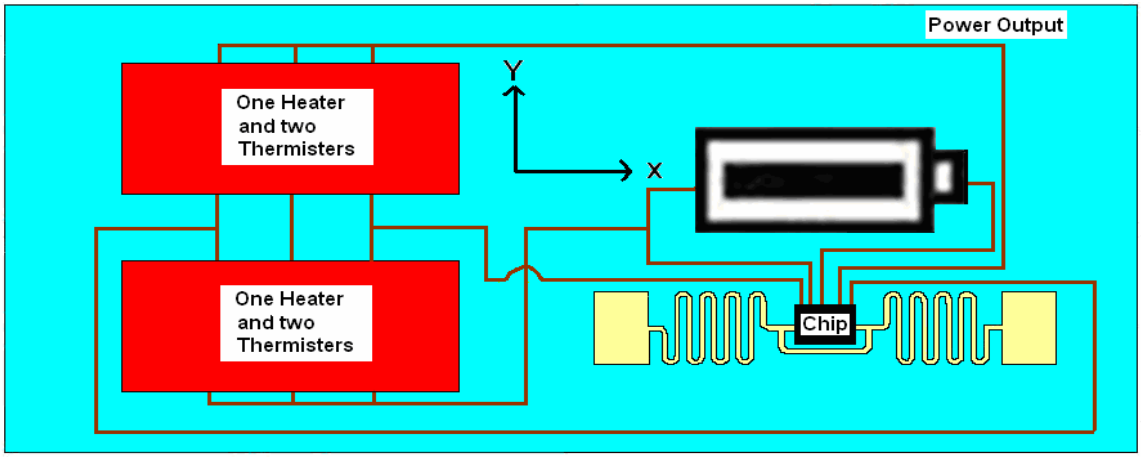

Fig.11. The result of design Step 10.

3 Simulation and Discussions

In this section we use ESI-CFD+ software package for simulation. Different geometries of heater, thermisters as well as the boundary conditions are applied first, and then we can obtain better results. The governing equations consist of the equations of continuity as:

$$\nabla \cdot \vec{u} = 0 \tag{1}$$

In addition, the conservation equations of mass, momentum, and energy can be expressed respectively as follows:

$$\frac{\partial \rho}{\partial t} + \nabla \rho \vec{u} = 0 \tag{2}$$

$$\frac{\partial \rho \vec{u}}{\partial t} + \nabla(\rho \vec{u}\vec{u}) = \nabla(\mu_{\mathrm{m}} \nabla \vec{u}) + \rho a - \nabla p \tag{3}$$

$$\rho c_{\mathrm{p}} \vec{u} \nabla T = k \nabla^2 T \tag{4}$$

where $\vec{u}$ is the velocity vector, t is the time, and ∇ is the standard spatial "grad" operator. ρ, μ_{m}, p, and a are density, dynamic viscosity, pressure, and acceleration, respectively, and c_{p}, T, and k are specific heat, temperature, and thermal conductivity of fluid, respectively. In addition, one has equation of state as:

$$\rho = p/RT \tag{5}$$

where R is the ideal gas constant. Let the width, thickness and length of SiO_2, thermisters and heater be respectively 4, 4 and 9 mm, and the components are equally spaced. The geometry definition of the accelerometer with semi-cylindrical and rectangular chambers are respectively shown in Fig. 12 (a) and (b), in which H = 19.7mm, W1 = 2mm, W2 = 4mm and W3 = 0.3mm. Firstly; the ratio (HSR1) of H to S1 is set as 19.7/9; the ratio (HSR2) of H to S2 is set as 19.7/8. In addition, the temperature of the package boundaries and the heater are respectively set as 300 and 400°K. The power generation of the heater is 50 W/m^2. The chamber is filled with carbon dioxide. Then the temperature differences of the thermal sensors versus acceleration (1G= 9.8 m/s^2) with cylindrical and rectangular chambers are shown in Fig. 13. One can see the sensitivity of the accelerometer by using the proposed semi-cylindrical chamber is almost equal to the conventional rectangular one.

On the other hand if the chamber is filled with xenon gas, then the sensitivities of the accelerometer with semi-cylindrical chamber are better than the rectangular one as shown in Fig. 14. The reason will be studied in the next paragraph.

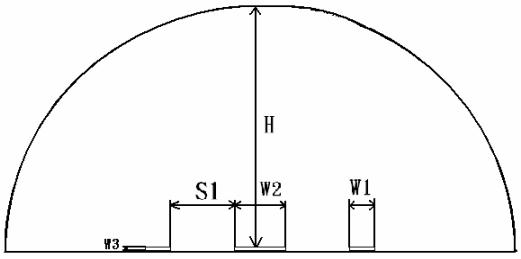

(a) Semi-cylindrical chamber.

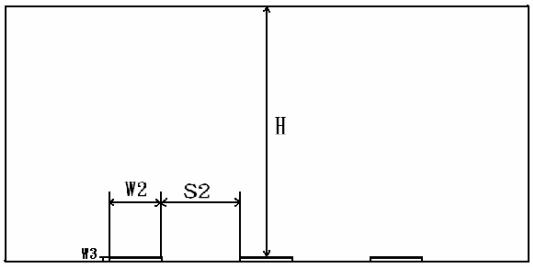

(b) Rectangular chamber.

Fig.12. The geometry definition of the accelerometer.

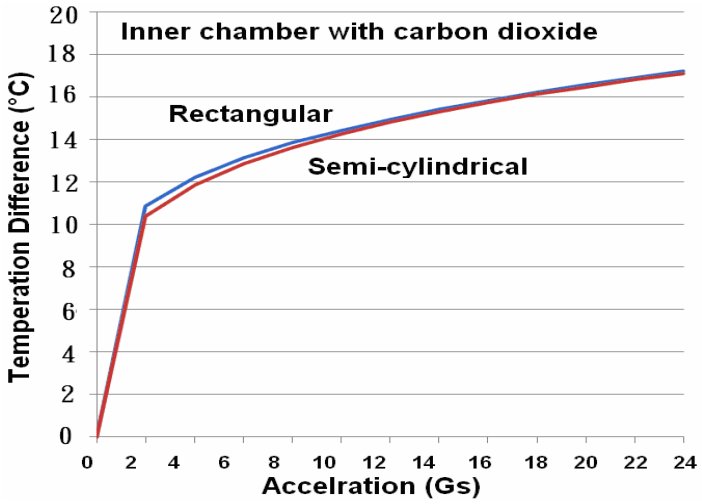

Fig.13. The temperature difference of the thermal sensors versus acceleration (in Gs) for semi-cylindrical and rectangular chambers filled with carbon dioxide.

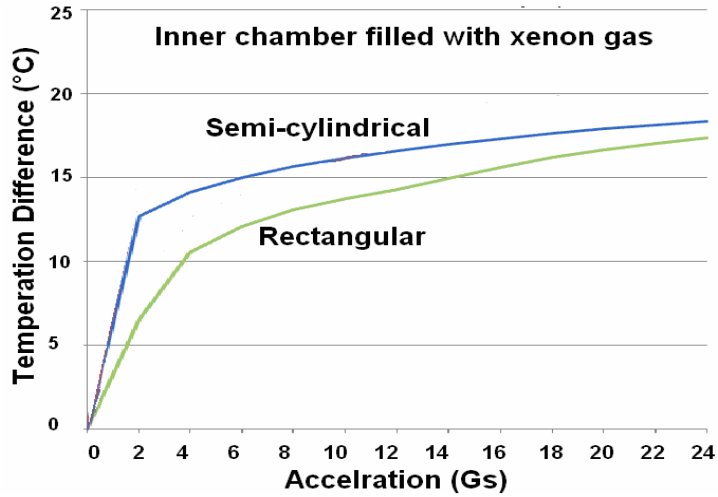

Fig.14. The temperature difference of the thermal sensors versus acceleration (in Gs) for semi-cylindrical and rectangular chambers filled with xenon gas.

In the following, only the semi-cylindrical and rectangular chambers filled with xenon gas are studied to find the reason behind Fig. 14. The results of 2D distributions of pressure, velocity vector, and temperature with Ax=0G for the semi-cylindrical and rectangular chambers are as in Figs. 15 (a), (b) and (c), and Figs. 16 (a), (b) and (c), respectively. One can see all the cases are in the reasonable symmetric conditions.

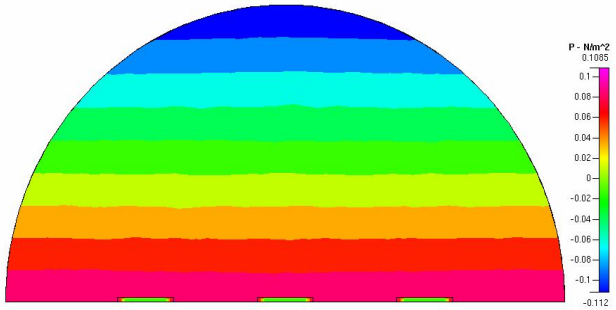

(a) Pressure.

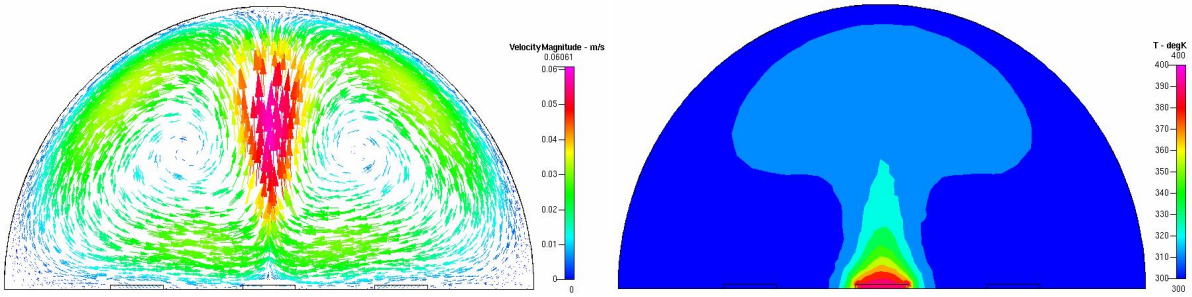

(b) Velocity vector. (c) Temperature.

Fig.15. The 2D distributions of pressure, velocity vector, and temperature for the semi-cylindrical chamber filled with xenon gas (Ax=0G).

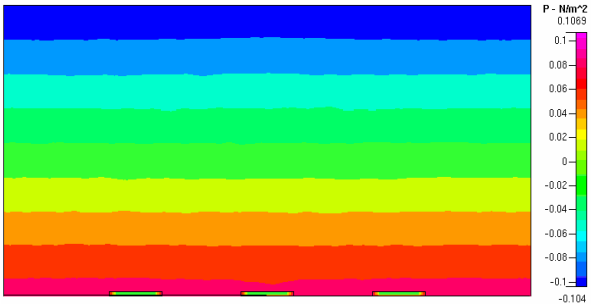

(a) Pressure.

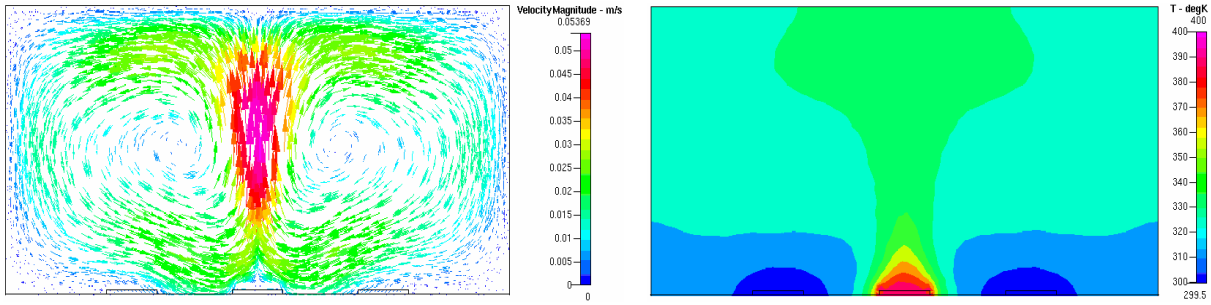

(b) Velocity vector. (c) Temperature.

Fig.16 The 2D distributions of pressure, velocity vector, and temperature for the rectangular chamber filled with xenon gas (Ax=0G).

The next case is for Ax=12G, Figs.17 (a), (b) and (c), and Figs.18 (a), (b) and (c) show the 2D pressure P, velocity vector and temperature distributions of the semi-cylindrical and rectangular chambers, respectively. Thus all the pressure P, velocity vector and temperature distributions are become unsymmetrical. One can see for the rectangular chamber there are a lot of gas turbulence effects along the boundaries and corners, and the hot gas can touch only a small part of the left thermal sensor, so the sensitivity is lowered as in Fig. 14.

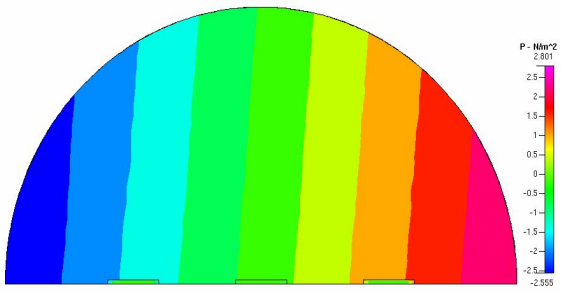

(a) Pressure.

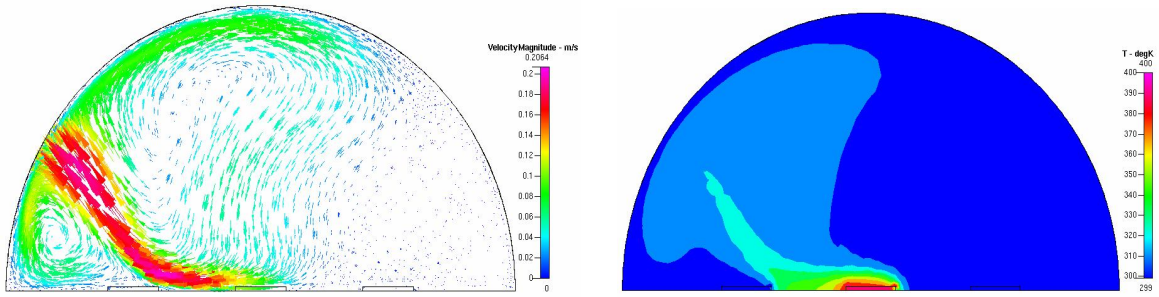

(b) Velocity vector. (c) Temperature.

Fig.17. The 2D distributions of pressure, velocity vector, and temperature for the semi-cylindrical chamber filled with xenon gas (Ax=12G).

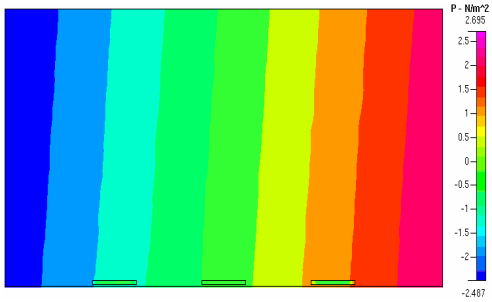

(a) Pressure.

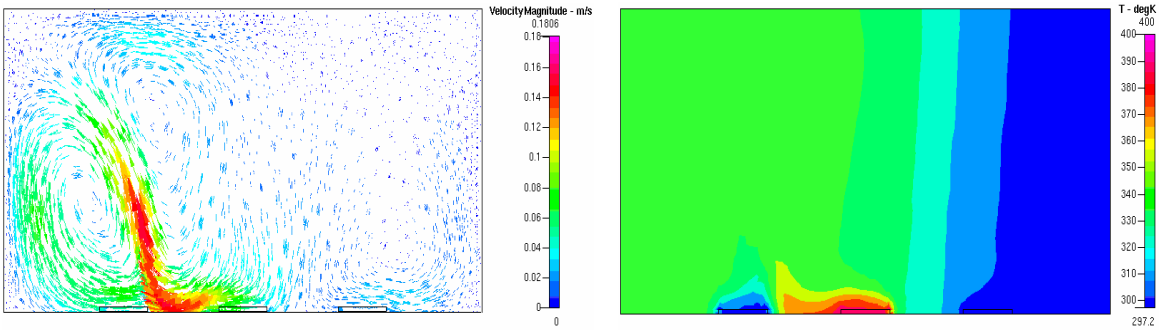

(b) Velocity vector. (c) Temperature.

Fig.18. The 2D distributions of pressure, velocity vector, and temperature for the rectangular chamber filled with xenon gas (Ax=12G).

If the acceleration is even larger i.e. Ax=24G, the 2D pressure P, velocity vector and temperature distributions of the semi-cylindrical and rectangular chambers are respectively as in Figs.18 (a), (b) and (c), and Figs.19 (a), (b) and (c). We can see for the rectangular chamber there are a lots of gas turbulence effects along the boundaries and corners, and the hot gas can hardly touch the left thermal sensor, so the sensitivity is still lowered as in Fig. 14.

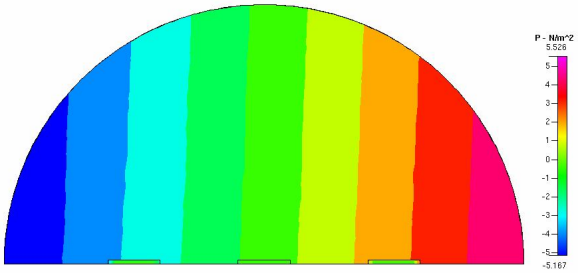

(a) Pressure.

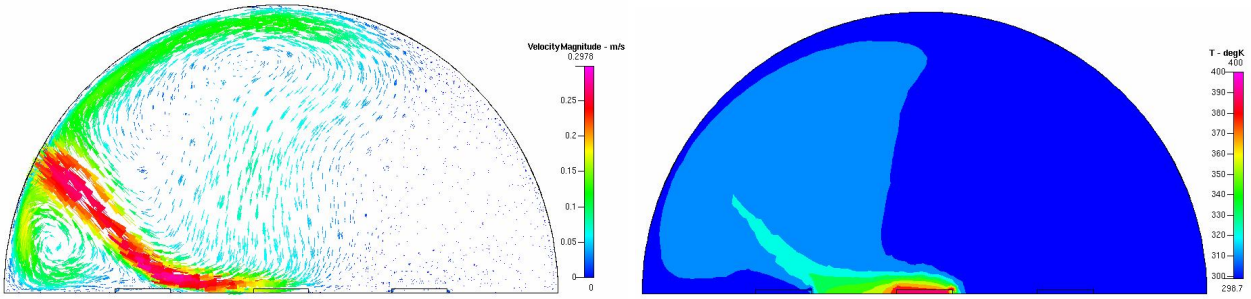

(b) Velocity vector. (c) Temperature.

Fig.18. The 2D distributions of pressure, velocity vector, and temperature for the semi-cylindrical chamber filled with xenon gas (Ax=24G).

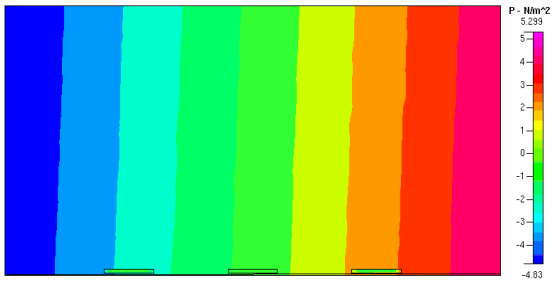

(a) Pressure.

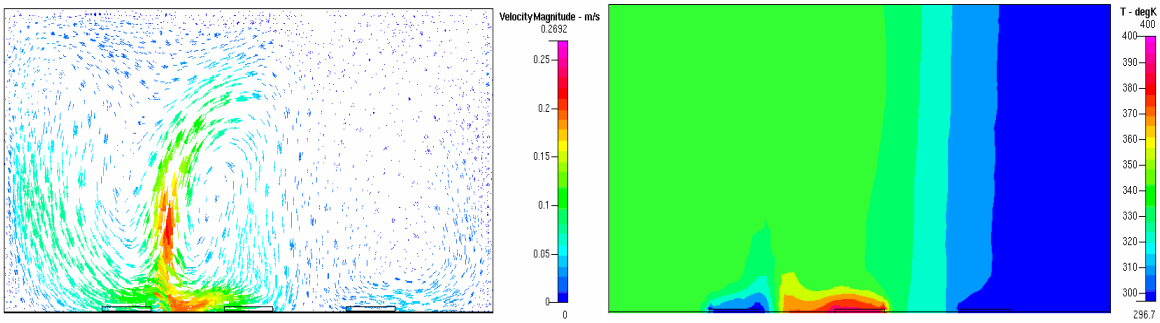

(b) Velocity vector. (c) Temperature.

Fig.19. The 2D distributions of pressure, velocity vector, and temperature for the rectangular chamber filled with xenon gas (Ax=24G).

From the above simulations one can see that the linearity properties of the curves are very good and without turbulence effect for larger accelerations (Ax), In addition, the results for the chamber filled with air and carbon dioxide are also included for comparison, which can prove the previous prediction that the sensitivity is better for the proposed accelerometer with semi-cylindrical chamber by using xenon gas to fill the chamber.

4 Conclusions

The major contributions of this paper are summarized as follows:

1. This is a new idea to make both heater and temperature sensors on the substrate directly without using the traditional floating structure, thus the proposed structure is simpler and cheaper for manufacturing, and much more reliable in large acceleration impact Gs.
2. This is a new idea to use plastic material as the substrate, the thermal isolation capability is better than the traditional silicon, thus the power dissipation and cost is lower for the new design.
3. This is a new idea to use the semi-cylindrical chamber, thus the gas flow field can settle down to the steady state

more quickly as well as without turbulent effect.
4. The fabrication process is in lower temperature, thus the cost can be reduced.
5. The chamber is filled with inert gas such as argon or xenon gas, thus the oxidizing effect produced by the traditional carbon dioxide or air can be avoided.
6. This is a new idea to evaporate either p-type amorphous (or poly) silicon or the K, J, E, and T type thermal piles on the plastic substrate as the temperature sensor.
7. This paper proposes a method to integrate the RFID tag with the thermal bubble accelerometer on the plastic substrate to make it be a wireless acceleration sensor.

Acknowledgements
This research was supported by National Science Council Taiwan, R.O.C. with contract NSC-93-2622-E-216-008-CC3.

References:
[1] L. M. Roylance and J. B. Angell, A Batch-Fabricated Silicon Accelerometer, *IEEE Transactions on Electron Devices*, Vol. 26, No.12, 1979, pp.1911-1917.
[2] L. Lin, R. T. Howe, and A. P. Pisano, Micro-Electromechanical Filters for Signal Processing, *J. Micro-Electromechanical System*, Vol. 7, No. 3, 1998, p. 286-294.
[3] Y. Zhao, A. P. Brokaw, M. E. Rebeschini, A. M. Leung, G. P. Pucci, and A. Dribinsky, Thermal Convection Accelerometer with Closed-loop Heater Control, US Patent NO：US 6,795,752 B1, September 2004.
[4] K. M. Liao, R. Chen and B. C. S. Chou, A Novel Thermal-bubble-based Micromachined Accelerometer, *Sensors and Actuators A: Physical*, Vol. 130-131, 2006, pp. 282-289.
[5] T. Mineta, S. Kobayashi, Y. Watanabe, S. Kanauchi, I. Nakagawa, E. Wuganuma and M. Esashi, Three-axis Capacitive Accelerometer with Uniform Axial Sensitivities, *J. Micromech. Microeng.* Vol. 6, No.4**,** 1996, pp. 431-435.
[6] L. C. Spangler and C. J. Kemp, ISAAC: Integrate Silicon Automotive Accelerometer, *Sens. Actuators,* Vol. 54, No. 1-3, 1996, pp. 523-529.
[7] L. M. Roylance and J. B. Angell, A Batch-Fabricated Silicon Accelerometer, *IEEE Trans. Electron. Devices***,** Vol. 26, No. 12, 1979, pp. 1911-1917.
[8] U. A. Dauderstadt, P. M. Sarro and S. Middelhoek, Temperature Dependence and Drift of a Thermal Accelerometer, *Sens. Actuators A,* Vol. 66**,** 1998, pp. 244-249.
[9] R. Dao, D. E. Morgan, H. H. Kries, D. M. Bachelder, Convective Accelerometer and Inclinometer, United States Patent US 5,581,034, REMEC, Inc., 1996.
[10] V. Milanovic, E. Bowen, N. Tea, J. S. Suehle, B. Payne, M. E. Zaghloul and M. Gaitan, Convection-based Accelerometer and Tilt Sensor Implemented in Standard CMOS, *MEMS Symp. Int. Mech. Eng. Exposition,* 1998, pp. 627-630.
[11] X. B. Luo, Z. X. Li, Z. Y. Guo and Y. J. Yang, Thermal Optimization on Micromachined Convective Accelerometer, *Heat Mass Transfer,* Vol. 38, No. 7-8, 2002, pp. 705-712.
[12] L. Lin, A. P. Pisano and V. P. Carey, Thermal Bubble Formation on Polysilicon Micro Resistors," *ASME J. Heat Transfer,* Vol. 120, No. 5, 1998, pp. 735-742.
[13] J. H. Tsai and L. Lin, Transient Thermal Bubble Formation on Polysilicon Micro-Resistors, *ASME J. Heat Transfer,* Vol. 124, No. 2, 2002, pp. 375-382.